

# Using *in situ* and Satellite Hyperspectral Data to Estimate the Surface Suspended Sediments Concentrations in the Pearl River Estuary

Qianguo Xing, Mingjing Lou, Chuqun Chen, and Ping Shi

**Abstract**—*In situ* remote sensing reflectance ( $R_{rs}$ ) collected during 2004–2006 and the planetary reflectance ( $R_p$ ) derived from EO-1/Hyperion image, are tested for estimating the surface total suspended matter (TSM), total inorganic particles (TIP) and water turbidity in the Pearl River Estuary (PRE). The *in situ* data show that the content of TIP and turbidity is proportional to the concentration of TSM which ranges from 6 mg/L to 140 mg/L. The band-subtraction of  $R_{rs}$  at 610 nm and 600 nm, [ $R_{rs}(610) - R_{rs}(600)$ ], and the subtraction of the 26th and 25th Hyperion bands (609.97 nm and 599.80 nm), [ $R_p(B26) - R_p(B25)$ ], are used in an exponential regression model to estimate the TSM concentrations, the mean relative errors between the estimated and measured TSM are 27.2% and 23.3%, respectively for  $R_{rs}$  and  $R_p$ , and the root mean square errors of estimation are 12.6 mg/L and 5.9 mg/L, respectively. This band-subtraction of two neighboring bands shows better performance than several popular single-band and band-combination models. This good performance may be mainly attributed to the band-subtraction of the two neighboring bands which improves the sensitivity of reflectance to suspended sediments by reducing the background impacts from water surface reflection and path radiance at the specific wavelengths. These methods and findings with the high spatial and high spectral resolution data may be used for the remote sensing of turbid estuary waters although further validation work with a wider range of TSM concentration may be necessary.

**Index Terms**—Hyperion, Pearl River Estuary, remote sensing, suspended sediments, total inorganic particles, total suspended matter, turbidity.

## I. INTRODUCTION

**I**N THE WORLD, the annual discharge of sediments to the oceans by the rivers is about 20 billion tons [1]. The suspension of sediments in water not only influences the aquatic ecology and biogeochemical cycles in estuaries [2], but also plays a key role in the forming and erosion of coastal land. Suspended sediments, full of organic and inorganic particles, are

the main source of total suspended matter, and control the turbidity of waters. Remote sensing is considered as an effective method of measuring the surface suspended sediments or the relevant water quality parameters and further evaluating the environment quality status [3]–[6].

At present, researchers are still trying to develop operational remote sensing algorithms to quantify suspended matter in coastal waters [7]. In addition to the impacts from the high content of color-producing components, e.g., micro-algae, colored dissolved organic matter, etc., the local characteristics of suspended sediments which are quite different in particle size and constituents in coastal waters, contribute to the optical characteristics of sediments and make the water color more optically complicated [8]. Moreover, there are still some shortcomings in the band configurations of current satellite imagers, e.g., due to the fact that the optical characteristics of Case-II waters are not fully understood yet, the spectral resolution and central wavelength settings of the current operational water color sensors like SeaWiFS (Sea-viewing Wide Field-of-view Sensor), MODIS (Moderate Resolution Imaging Spectroradiometer), are not adequate for coastal waters. Thus, it is quite difficult to develop an operational algorithm for the retrieval of suspended sediments, especially for estuary waters. Previous studies show that suspended matter retrieval models established by different researchers are highly dependent on local characteristics of study area where the data are collected, e.g., single band model, band ratio [9], band combination [10], [11], and reflectance peak area model [12].

In this study, hyperspectral data is adopted to explore the potential of remote sensing in estimating the suspended sediments, the content of inorganic particles, and turbidity in the Pearl River Estuary, China. *In situ* collected data will be used to study the characteristics of remote sensing reflectance corresponding to suspended sediments and to evaluate the retrieval models, and the optimum model will be tested with Hyperion image data collected by satellite EO-1 (Earth Observing 1) for further application.

## II. METHODS AND DATA

### A. Study Area

The Pearl River is the largest river in south China with a mean annual runoff of up to 336 billion cubic meters, and it has three branch rivers—Xijiang, Beijiang and Dongjiang. The Xijiang river, the trunk of the Pearl River, flows 2,197 kilometers before draining into the South China Sea, and has 77% of the total runoff of the Pearl River. The three rivers meet at the Pearl River

Manuscript received August 25, 2012; revised October 22, 2012 and December 03, 2012; accepted December 20, 2012. Date of publication January 30, 2013; date of current version May 13, 2013. This work was jointly supported by the National Natural Science Foundation of China (No. 40976106), and the CAS/SAFEA International Partnership Program for Creative Research Teams. (Corresponding author: Q. Xing.)

Q. Xing, M. Lou, and P. Shi are with the Yantai Institute of Coastal Zone Research, Chinese Academy of Sciences, Yantai 264003, China (e-mail: qgxing@yahoo.com).

C. Chen is with the South China Sea Institute of Oceanology, Chinese Academy of Sciences, Guangzhou 510301, China.

Color versions of one or more of the figures in this paper are available online at <http://ieeexplore.ieee.org>.

Digital Object Identifier 10.1109/JSTARS.2013.2238659

TABLE I  
HYPERION AND THE OTHER TWO ON-ORBIT HYPERSPECTRAL IMAGERS

Sensor	HYPERION	HSI	HICO
Starting year	2002	2008	2009
Platform	EO-1	HJ-1A	ISS
Orbit	Sun-synchronous circular orbit	Quasi- Sun-synchronous circular orbit	circular orbit
Altitude, km	705	650	343
Swath width, km	7.7	50	42
Revisit cycle, day	5~16*	4~31*	1~3*
Spectral range, nm	400~2500	450~950	360~1080
Number of bands	220	115	128
Spectral resolution, nm	10	5	5.7
Spatial resolution, m	30	100	90
Ratio of S/N	<200	50~100	>200

\* With side-looking mode.

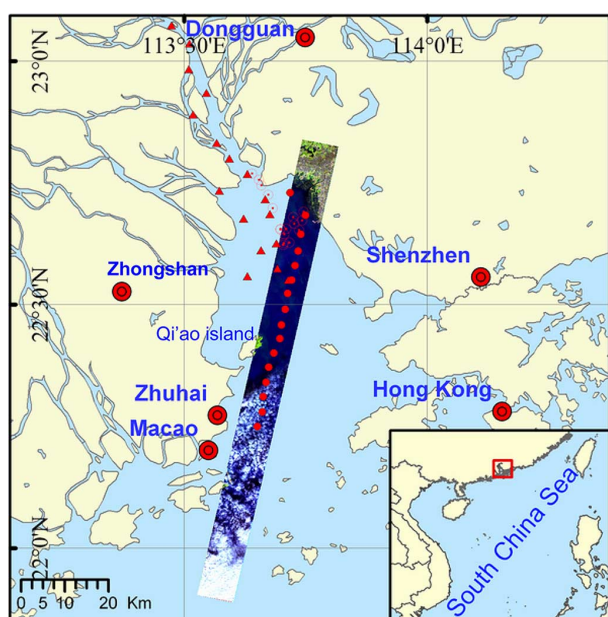


Fig. 1. Study area and sampling stations at the Pearl River Estuary (▲, GMRMC routine stations, on May 18, 2004, May 23, 2006 and Aug., 21, 2006; ●, stations of sampling simultaneously with satellite over-fly, on Dec. 6, 2006, i.e., S1, S2 to S16 in turn from the upper to the lower of the image; ○, stations of cruise on Dec. 21, 2006).

Delta formed of the silt deposits at the river estuary (the Pearl River Estuary, PRE), where they flow into the South China Sea through eight outlets and form the network of rivers in this area. As relevant records, the average annual discharge of sediments is about 75, 290, 000 t [13]. The estuary is very important for transportation, fisheries and the habitat of rare species such as Chinese white dolphin. The Pearl River delta is highly populated and industrialized especially in the latest three decades, and the PRE water status is worsening due to the impacts brought by human activities. Many management projects are launched by local governments to recover the water environment and make the water more clean. The study area is shown in Fig. 1.

### B. Sampling Surveys

From 2004 to 2006, five cruises were carried out in the PRE to collect the data of remote sensing reflectance and water quality data. A semi-simultaneous sampling campaign was carried out

during the period of 9:30 AM–12:00 AM with the overpass of the EO-1/Hyperion at 10:37 AM on Dec. 6, 2006. The Hyperion on board the satellite of EO-1 is the first spaceborne hyperspectral imager (<http://www.eo1.usgs.gov/hyperion.php>), it has high radiometric accuracy, and can monitor an area of 7.5 km × 100 km per image with a ~10 nm spectral resolution of 220 bands (from 0.4 to 2.5 μm) and with a 30-meter spatial resolution, which makes its product more suitable for monitoring the small-scale fine spatial distribution of water parameters [14], [15] than other product with coarse spatial resolution [16]–[18]. As shown in Table I, the characteristics of Hyperion are compared with the sensors of Hyperspectral Imager for the Coastal Ocean (HICO) on board the International Space Station (ISS) and the HyperSpectral Imager (HSI) on board HJ-1A [19].

All the cruises were carried out with the ship 908# from Guangzhou Marine Resources Monitoring Center (GMRMC), and the *in situ* water sampling and laboratory analysis were according to the China National Standard (GB17378.7-1998). The remote sensing reflectance ( $R_{rs}$ ) and turbidity were measured *in situ* by portable instruments [20], [21]. Water samples were collected at the depth of 0.5 m below the water surface and kept in cool and dark containers for further laboratory analysis that day. 1 L of water samples were filtered with the dried (at 60°C) and preweighted 0.45 μm polycarbonate Whatman membrane filters (initial weight of membrane filter,  $W_0$ , mg), and the filters were dried with the temperature of 60°C until their weights ( $W_1$ , mg) were constant, then we calculated the mass of filtered sediments ( $W_1 - W_0$ , mg) and the concentration of total suspended matter (TSM, mg/L); finally, the dried filters were put in preweighted pots ( $W_{01}$ , mg) and combusted at 450°C for 6 hrs to remove the combustible organic matter and the pots were weighed ( $W_{02}$ , mg), and we had the mass of total inorganic particles (TIP,  $W_{02} - W_{01}$ , mg) and their concentrations (mg/L). The general information about the cruises and data is shown in Fig. 1 and Table II.

### C. Processing of *in situ* Spectra Data and Analysis

The *in situ* collected  $R_{rs}$  spectra are bin-averaged to provide continuous spectra with a 10 nm bandwidth, which is close to the band configurations of Hyperion. If random band-combination is used to investigate the relationship between the suspended sediments and the tens (or hundreds) of bands, the workload will be huge and the result is usually ambiguous. The algo-

TABLE II  
SAMPLING SURVEYS IN THE PEARL RIVER ESTUARY AND DATA SUMMARY

Date	Avg.TSM (S.D.)	Avg.Turbidity (S.D.)	TIP	Sampling Sites
May 18, 2004	53.2 (27.6)	52.5 (31.1)	-	▲
May 23, 2006	22.6 (15.3)	27.8 (15.3)	-	▲
Aug. 21, 2006	49.0 (35.8)	37.5 (27.5)	-	▲
Dec. 06, 2006	25.0 (11.3)	-	21.6 (10.2)	●
Dec. 21, 2006	34.0 (28.4)	-	31.7 (26.3)	⊙
Averages (S.D.)	39.1 (28.5)	42.9 (28.9)	26.7 (20.3)	

“-” indicates no data collected.

riethms with single band and the first or second order derivatives are arithmetically simple and relatively clear in a bio-physical view. According to the preliminary results from Xing *et al.* [22], the first order derivative of  $Rrs$  (1) has better performance than the second order derivative in estimating the sediments concentrations in the PRE, especially at 605 nm.

$$Rrs^{1st} = \frac{Rrs_{n+1} - Rrs_n}{\lambda_{n+1} - \lambda_n} \quad (1)$$

where  $n$  is the band number,  $\lambda$  is the wavelength,  $Rrs^{1st}$  is the first-order derivative (a finite difference approximation of the derivative with respect to wavelength), and its central wavelength is  $(\lambda_{n+1} + \lambda_n)/2$ . In our practice, the central wavelengths are fixed, i.e.,  $(\lambda_{n+1} - \lambda_n)$  is constant, so, the model is substituted by the band-subtraction of the two neighboring bands.

Li *et al.* [11] proposed a popular two-band combination algorithm for the retrieval of suspended sediments in the Yangtze River Estuary, China. The input variable includes the bands of 550 nm and 670 nm with the form of  $[Rrs(550) + Rrs(670)]/[Rrs(550)/Rrs(670)]$  (Li model). A remote sensing model of TSM using MODIS data is proposed by Dennis K. Clark for the most popular ocean color remote sensing software of *SEADAS* ([http://www.oceancolor.gsfc.nasa.gov/forum/oceancolor/topic\\_show.pl?tid=1559](http://www.oceancolor.gsfc.nasa.gov/forum/oceancolor/topic_show.pl?tid=1559)), in which a fifth-order polynomial function with the input variable of  $[Rrs(440) + Rrs(490)]/Rrs(550)$  is used (Clark model). The two models will be tested with the *in situ*  $Rrs$  data for comparisons.

Root mean square error (RMSE) and relative error (RE), as (2) and (3), will be used to evaluate the accuracy of different models in this study:

$$RMSE = \sqrt{\frac{\sum_{i=1}^n (C_{estimated} - C_{measured})^2}{n}}, \quad (2)$$

$$RE = \frac{|C_{estimated} - C_{measured}|}{C_{measured}} \times 100\%, \quad (3)$$

where  $C_{measured}$  and  $C_{estimated}$  are the concentration of TSM measured *in situ* and estimated by model, respectively.

#### D. Processing of Hyperion Image and Analysis

For the Hyperion image data collected on December 6, 2006, it is smoothed at first with a window of  $3 \times 3$  pixels to reduce possible noises caused by detectors, and then the pixels of band 150 (1648.90 nm) with the DN value lower than 100

(1.25 W/(m<sup>2</sup> · sr · μm)) are classified as water. For the pixels of water, the DN values of each band for water are converted to radiance on the basis of the coefficients of gains and offsets, and further converted to the planetary reflectance ( $Rp$ ) to remove the impacts from the solar irradiance due to the changes in the sun's elevation and the sun-earth distance [23], [24], as (4):

$$Rp(\lambda) = \frac{\pi \cdot L(\lambda) \cdot d^2}{F_0(\lambda) \cdot \cos \theta} \quad (4)$$

where  $L(\lambda)$  is the spectral radiance recorded by the sensor,  $d$  is the earth-sun distance in astronomical units,  $F_0(\lambda)$  is the mean solar exoatmospheric irradiance, and  $\theta$  is the solar zenith angle. The latter three parameters can be calculated or found using look-up tables (<http://www.eol.usgs.gov/hyperion.php>).

As shown in Fig. 1, among the 16 stations, the first station S1 is out of the Hyperion image because the site was not accessible on Dec. 6, 2006, and the last five stations at the lower of the image were heavily impacted by clouds. So, the data for the 11 stations from S2 to S12 are used for analysis with the image data.

### III. RESULTS AND DISCUSSION

#### A. TSM, TIP and Turbidity

According to the collected data during these cruises, the content of TSM has a wide range from 6 to 140 mg/L, and its averaged content (with the standard deviation) is 39.1 mg/L ( $\pm 28.5$  mg/L), which is close to other observation results [25] at this area. As shown in Fig. 2, the water turbidity and the total inorganic matter (TIP) are proportional to the content of TSM, and the averaged ratio of TIP to TSM is 87.3% ( $\pm 5.9\%$ ). The good linear relationship between them makes it possible to select one of them as their proxies in actual remote sensing applications, e.g., TSM in this study. In this case, the turbidity data were collected in the months of May and August (wet season), and the TIP data in December (dry season); so, the linear relationship between TSM and them may be different in different seasons. More data can be collected in different seasons at different area to investigate this issue and find the robust relationship. It should be noted that the turbidity depends on not only the concentration of particles (TSM or TIP) but also the size, composition of particle matter and so on [26]. The relatively more irregular relationship between turbidity and TSM (see the scattering plot of Fig. 2) also suggests that it may need a specific retrieval model

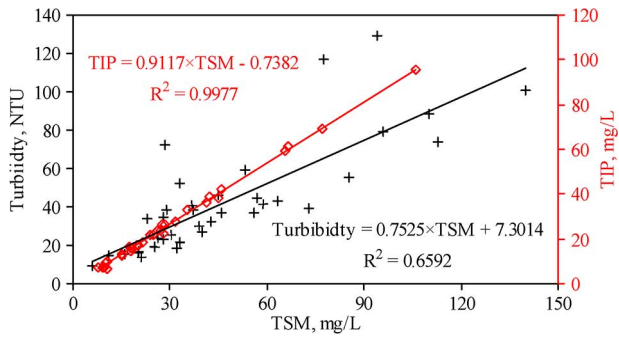


Fig. 2. The relationship between TSM and TIP, turbidity in the PRE. (TSM vs. Turbidity is shown in black symbol “+”, and TSM vs. TIP in red diamonds).

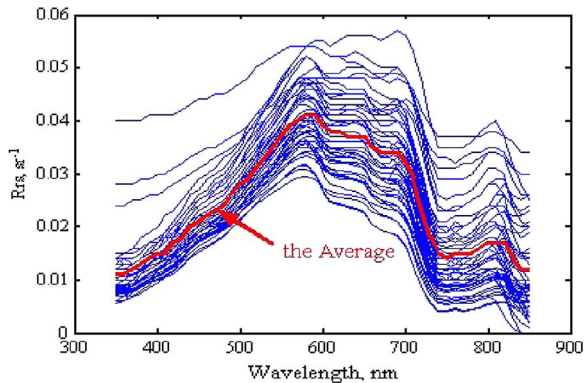


Fig. 3. *In situ* collected remote sensing reflectance ( $R_{rs}$ ) spectra of the PRE waters.

for turbidity rather than a simple TSM-based model [7] although we don't intend to do so in this study.

### B. Spectra of Remote Sensing Reflectance

Usually, because of the strong light absorption by water molecules, the  $R_{rs}$  of water is low and has small fluctuations at long wavelengths. However, in this study, as in Fig. 3, the *in situ* collected  $R_{rs}$  varies sharply even at longer wavelengths (750–850 nm), which may be partly ascribed to the difference in the suspended particles concentrations and their different optical characteristics. In the study area, the network of abundant rivers provide many sources of sediments from the upper reach, and the human activities also disturb the estuary bed and lead to the re-suspension of bed sediments, e.g., dredging, ships' passing-by. The different sources of sediments vary in particle size and constituents [25]. Sky conditions changed greatly during the cruises, the empirical method to remove the Fresnel effects of sky light [20] is not adequate and thus bring some errors, which will also contribute to the variations of  $R_{rs}$ .

### C. Estimating TSM Using *in situ* Hyperspectral Data

Correlation analysis was made between TSM and the single bands, the first-order and second-order derivatives as by Xing *et al.* [22], the results (Fig. 4) suggest that the first derivatives at several wavelengths have better correlation relationship with the content of suspended sediments, especially at 605 nm, i.e., [ $R_{rs}(610) - R_{rs}(600)$ ]. As previously mentioned, the first-order

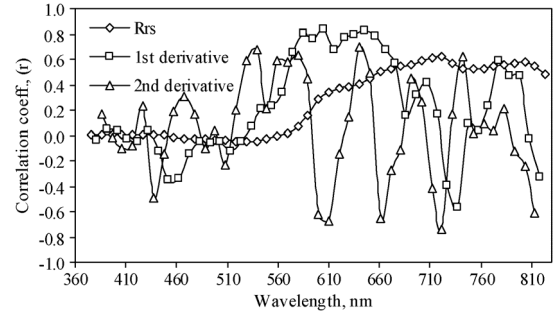


Fig. 4. Correlation between TSM and single bands of  $R_{rs}$ , the first and second order derivatives.

derivative is another form of band subtraction. Results show that, the band subtraction of [ $R_{rs}(610) - R_{rs}(590)$ ] is close to [ $R_{rs}(610) - R_{rs}(600)$ ]; the single bands at longer wavelength (>650 nm) is more correlated to TSM (correlation coefficient,  $r > 0.4$ ), especially at about 720 nm and 800 nm, and 480 nm seems to have no correlation with TSM ( $r \approx 0$ ), so  $R_{rs}(720)$  is normalized by  $R_{rs}(480)$  as [ $R_{rs}(720) - R_{rs}(480)$ ], a different band combination of subtraction; in addition, the two-band combination of [ $(R_{rs}(550) + R_{rs}(670)) / (R_{rs}(550) / R_{rs}(670))$ ] proposed by Li *et al.* [11] and the above mentioned three band combination of [ $(R_{rs}(440) + R_{rs}(490)) / R_{rs}(550)$ ] are also tested for comparisons. The relationships are shown as in Fig. 5. Statistical models are developed by linear or nonlinear regression, and their performances are shown in Table III. In general, the band-subtraction combination in the form of first-order derivative at 605 nm have the best performance with the lowest mean RE and RMSE; the three band combination proposed by Clark (Fig. 5(f)) fails in the turbid PRE waters; maybe due to the fact that the two-band combination proposed by Li *et al.* [11] (Fig. 5(e)) was also developed on the basis of data collected at the estuary (Yangtze River), the model of Li *et al.* [11] performs well at the Pearl River Estuary, and its estimation accuracy is comparable to that of the single band of  $R_{rs}(720)$  (Fig. 5(c)), although they are not so good as the ones here in the form of band subtraction. Tassan [10] developed a model for the retrieval of suspended sediments concentration in the Gulf of Naples (Mediterranean Sea), and this model was optimized by Tang *et al.* [27] and it worked well at the Yellow Sea and the East China Sea, however it seems to be not suitable for the Pearl River Estuary waters: the determination coefficients in the regression between TSM and the band-combination index ( $R^2 = 0.2513$ ), is even much lower than that of the single band model (Fig. 5(c)) or the model of Li *et al.* [11] (Fig. 5(e)). The good performance of the band-subtraction especially of two neighboring bands can be mainly ascribed to its characteristic ability to remove the flat-curve-like spectral background impacts, e.g., Fresnel effect [21]. In field work, the measured upwelling radiance above water ( $L_u$ ) is the sum of the reflected sky light ( $L_{sky}$ ) and the water-leaving radiance ( $L_w$ ), i.e.,  $L_u = L_{sky} + L_w$ . When the upwelling radiance is normalized by downwelling irradiance ( $E_d$ ), we can get:  $L_u/E_d = L_{sky}/E_d + R_{rs}$ . The curve of  $L_{sky}/E_d$  is close to a flat line at longer wavelength (600 nm and above), so,

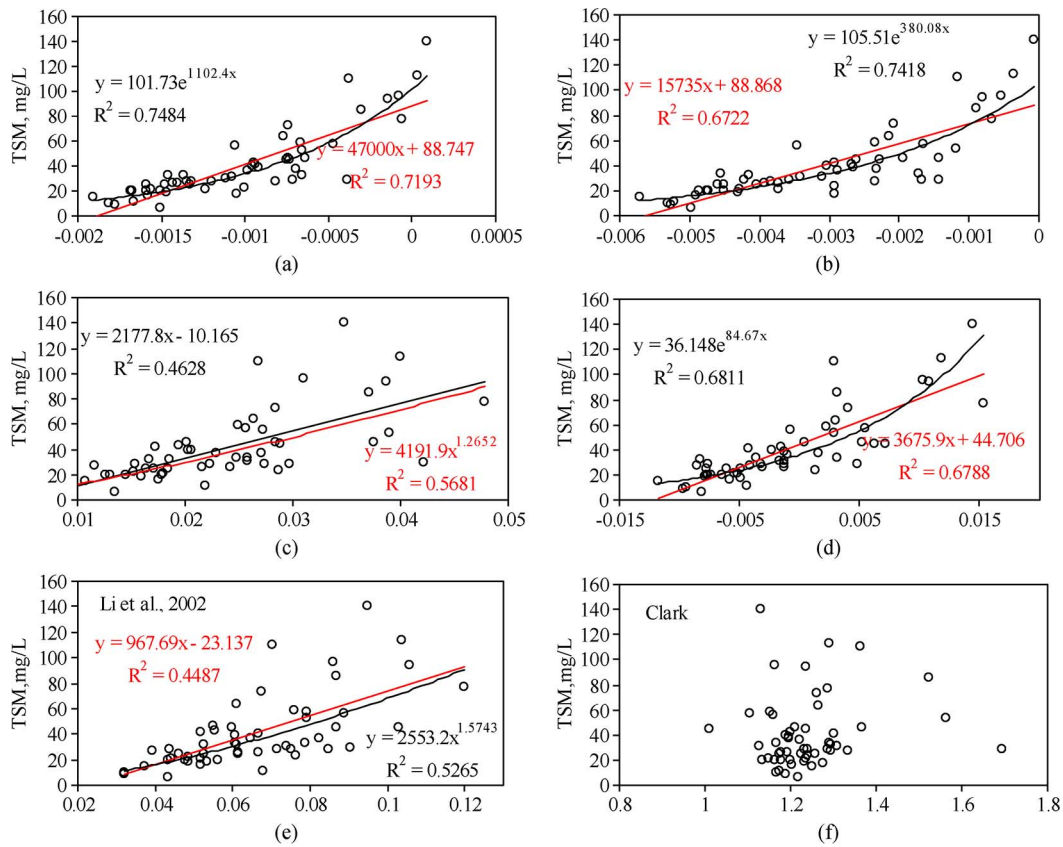


Fig. 5. The relationship between TSM and the single  $Rrs$  band and band combinations (number of data points,  $n = 55$ ). (Statistical models are established by linear or nonlinear regression for different input variables of  $Rrs$ : linear model is in red color and nonlinear in black.) (a)  $Rrs(610) - Rrs(600)$ ; (b)  $Rrs(610) - Rrs(590)$ ; (c)  $Rrs(720)$ ; (d)  $Rrs(720) - Rrs(480)$ ; (e)  $[Rrs(550) + Rrs(670)]/[Rrs(550)/Rrs(670)]$ ; (f)  $[Rrs(440) + Rrs(490)]/Rrs(550)$ .

TABLE III  
TSM RETRIEVAL MODELS AND PERFORMANCES

x	Algorithms (y, TSM)	$R^2$	Mean RE, %	RMSE, mg/L
$Rrs(610) - Rrs(600)$	$y = 101.73 \times e^{1102.4x}$	0.7484	27.2	12.61
	$y = 47000x + 88.747$	0.7193	35.3	15.03
$Rrs(610) - Rrs(590)$	$y = 105.51 \times e^{380.08x}$	0.7418	27.5	13.80
	$y = 4191.9x^{1.2652}$	0.5681	37.1	21.28
$Rrs(720)$	$y = 2177.8x - 10.165$	0.4628	41.4	20.79
	$y = 36.148 \times e^{84.67x}$	0.6811	30.6	16.29
$[Rrs(550) + Rrs(670)] / [Rrs(550) / Rrs(670)]$	$y = 967.69x - 23.137$	0.4487	39.7	21.99
	$y = 2553.2x^{1.5743}$	0.5265		

band subtraction may reduce the effects of sky light's Fresnel reflection at the water surface.

#### D. Mapping of the Surface Suspended Sediments With Hyperion/EO-1

For Hyperion image data, the 26th and 25th bands (B26 and B25), i.e., the bands with the wavelength of 609.97 and 599.80 nm, respectively, have the wavelength very close to that in Fig. 5(a), and the corresponding first-order derivative can be written as  $[R_p(B26) - R_p(B25)]$ . As in Fig. 6(a), an exponential function similar to that in Fig. 5(a) fit well the relationship between the *in situ* TSM and  $[R_p(B26) - R_p(B25)]$  (see (5)), and the difference between the estimated TSM and the *in situ* measured is small: the mean RE is 23.3%, and the RMSE 5.9

mg/L. Because of the atmospheric effects,  $R_p$  at the top of atmosphere (TOA) is linked but quite different to  $Rrs$  just above the water surface.  $Rrs$  is defined as the ratio of water-leaving radiance ( $L_w$ ,  $mW/(cm^2 \cdot \mu m \cdot sr)$ ) to downwelling irradiance just above the surface ( $Ed$ ,  $mW/(cm^2 \cdot \mu m)$ ) [28], while  $R_p$  is the ratio of upwelling radiance ( $L$ ) recorded by satellite sensor to the solar irradiance (see (4));  $L$  is the sum of the attenuated  $L_w$  by the atmosphere and the atmospheric path radiance ( $L_p$ ), and  $Ed$  is the sum of the attenuated solar irradiance and the atmospheric path irradiance. So, when band subtraction is applied to  $R_p$ , the atmospheric absorption and scattering will affect the actual empirical retrieval model. Atmospheric correction has been done with Hyperion hyperspectral image data [14], [15], however, the operational method of atmospheric

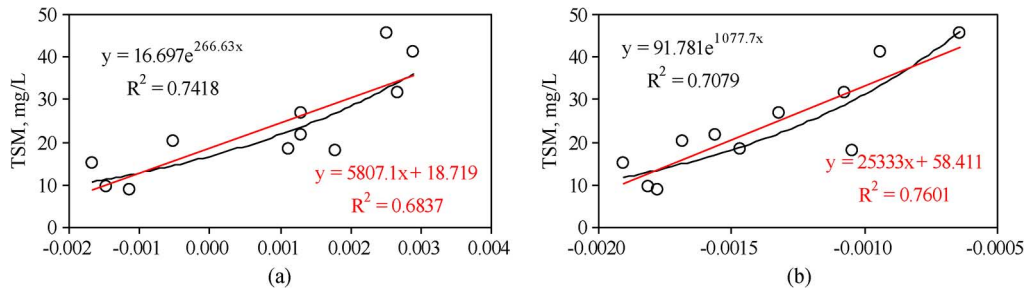


Fig. 6. The relationship between TSM and band subtraction index: a,  $[R_p(B26) - R_p(B25)]$ , and b,  $[R_{rs}(610) - R_{rs}(600)]$ . (B26 is for the band at 609.97 nm, B25 for 599.80 nm, and the wavelength corresponding to  $[R_p(B26) - R_p(B25)]$  is also 605 nm, i.e.,  $R_p^{1st}$  at 605 nm).

correction for turbid coastal waters remote sensing is still a question. Although no atmospheric correction was done with the original Hyperion data, the exponential model in Fig. 6(a) is still comparable to that in Fig. 6(b) which is based on the *in situ*  $R_{rs}$  spectra. According to the atmospheric effects, the 10-nm-resolution spectrum of atmospheric path radiance is relatively flat at 600 nm or 610 nm, so, the band subtraction of two bands especially in neighborhood can remove most of the effects caused by atmospheric path radiance. This application supports the idea that the first-order derivative may be used to reduce atmospheric impacts [29]. The first order derivative approach can also be used to estimate the surface chlorophyll [21], although it may be not the most appropriate one.

$$[TSM] = a \cdot e^{b \cdot (R_p(B26) - R_p(B25))} \quad (5)$$

where  $a$  and  $b$  are coefficients calibrated in practice, i.e., 16.697 and 266.63, respectively in this study.

On the basis of the (5) and the linear relationship between TSM and TIP, turbidity, the three parameters in the PRE are estimated by Hyperion image data, as shown in Fig. 7; although the image is not wide enough, the result still shows the sharp spatial variations in the surface suspended sediments, and also indicates the area with relatively higher content of suspended sediments at the southwestern part of the PRE, especially near the Qi'ao island (see its position in Fig. 1). This distribution pattern of surface suspended sediments is consistent with the common sense that the southward turbid current at PRE turns west under the Coriolis force [30]. The Advanced Land Imager (ALI) also on board EO-1 was used to study the turbid waters of Maodaomen waterway in the PRE [31], but it didn't cover the area of Hyperion image in our study. These studies can give a more full spatial review of the PRE turbid waters.

#### IV. CONCLUSIONS AND PERSPECTIVES

The first-order derivative has the ability to remove the spectral background caused by sky light and atmospheric path radiance at certain wavelengths. In practice, due to the fixed band settings, the first-order derivative spectra can be simplified as a band combination of band subtraction of two neighboring bands. For the suspended sediments concentration (TSM) which ranges 6–140 mg/L at the Pearl River Estuary, China, the exponential retrieval model of using the first-order derivative of reflectance at 605 nm (band subtraction of two neighboring bands) is proposed. The model is applied to the *in situ* remote sensing

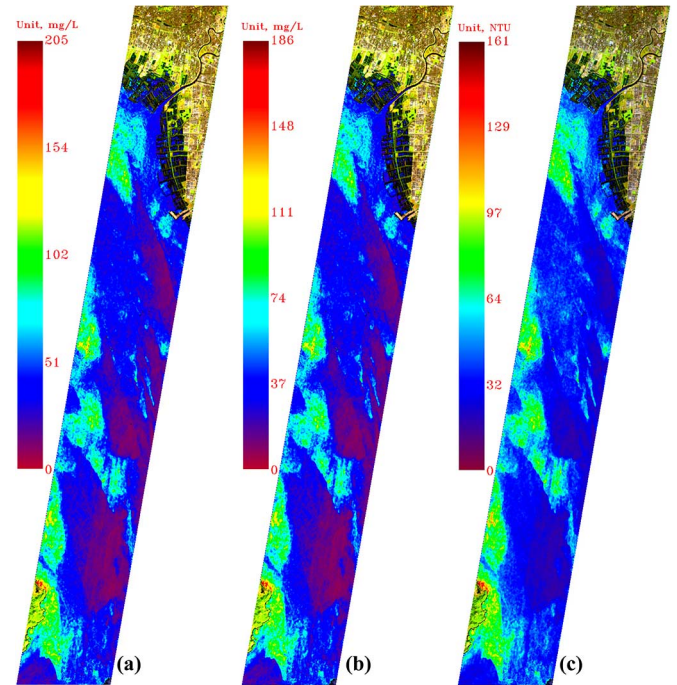


Fig. 7. The distribution of TSM, TIP and turbidity retrieved from Hyperion image. The spatial distributions of TSM, TIP and Turbidity are very close because of the linear relationship between these three parameters (note the difference in color bar). (a) TSM; (b) TIP; (c) Turbidity.

reflectance and the Hyperion planetary reflectance, both satisfying performances in estimating the TSM are achieved: the mean RE is less than 30%, and RMSE lower than 13 mg/L. These results suggest that the method of first-order derivative (or, subtraction of two neighboring bands) may be used for estimating the suspended sediments in coastal turbid waters, and that the hyperspectral image data like Hyperion is applicable in coastal water remote sensing.

In this case, the index of first-order derivative is used to estimate suspended sediments, and the index at 605 nm has a good performance; however, it should be kept in mind that, there may be more potential wavelengths suitable for the retrieval of suspended sediments, e.g., 585 nm, 645 nm etc. The first-order derivative can deal with the atmospheric path radiance, and we expect for its new forms which be improved to handle the atmospheric transmittance and make the spaceborne remote sensing model more robust. And, for further application of this model to other more turbid estuary waters, validation

work need to be done with a larger range of TSM concentration than the 6–140 mg/L at the Pearl River Estuary.

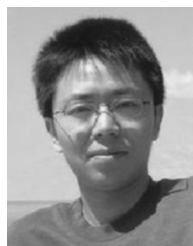
#### ACKNOWLEDGMENT

The authors are grateful to Dr. Shilin Tang, Dr. Heyin. Shi and Mr. Jinkun Yang for their help in sampling work. The authors also thank the anonymous reviews for their insightful comments and help to the manuscript.

#### REFERENCES

- [1] J. D. Milliman and J. P. M. Syvitski, "Geomorphic/tectonic control of sediment discharge to the ocean: The importance of small mountainous rivers," *J. Geol.*, vol. 100, no. 5, pp. 325–344, Sep. 1992.
- [2] A. Turner and G. E. Millward, "Suspended particles: Their role in estuarine biogeochemical cycles," *Estuar. Coast. Shelf. S.*, vol. 55, no. 6, pp. 857–883, 2002.
- [3] J. C. Ritchie, F. R. Schiebe, and J. R. McHenry, "Remote sensing of suspended sediment in surface water," *Photogramm. Eng. Remote. S.*, vol. 42, no. 12, pp. 1539–1545, Dec. 1976.
- [4] D. G. Goodin, L. Han, R. N. Fraser, D. C. Rundquist, W. A. Stebbins, and J. F. Schalles, "Analysis of suspended solids in water using remotely sensed high resolution derivative spectra," *Photogramm. Eng. Remote. S.*, vol. 59, no. 4, pp. 505–510, 1993.
- [5] C. Chen, S. Tang, Z. Pan, H. Zhan, M. Larson, and L. Jönsson, "Remotely sensed assessment of water quality levels in the Pearl River Estuary, China," *Mar. Pollut. Bull.*, vol. 54, no. 8, pp. 1267–1272, Aug. 2007.
- [6] J. Chen and W. Quan, "Using LandsatTM imagery to estimate nitrogen and phosphorus concentration in Taihu Lake, China," *IEEE J. Sel. Topics. Appl. Earth Observ. Remote. Sens.*, vol. 5, no. 1, pp. 273–280, Feb. 2012.
- [7] S. Ouillon, P. Douillet, A. Petrenko, J. Neveux, C. Dupouy, J. M. Froidefond, S. Andréfouët, and A. Muñoz-Caravaca, "Optical algorithms at satellite wavelengths for total suspended matter in tropical coastal waters," *Sens.*, vol. 8, no. 7, pp. 4165–4185, Jul. 2008.
- [8] R. P. Stumpf and J. R. Pennock, "Calibration of a general optical equation for remote sensing of suspended sediments in a moderately turbid estuary," *J. Geophys. Res.*, vol. 94, no. C10, pp. 14363–14371, 1989.
- [9] D. Doxaran, R. C. N. Cherukuru, and S. J. Lavender, "Use of reflectance band ratios to estimate suspended and dissolved matter concentrations in estuarine waters," *Int. J. Remote. Sens.*, vol. 26, no. 8, pp. 1763–1769, Apr. 2005.
- [10] S. Tassan, "Local algorithm using SeaWiFS data for the retrieval of phytoplankton, pigments, suspended sediment and yellow substance in coastal waters," *Appl. Opt.*, vol. 33, no. 12, pp. 2369–2378, 1994.
- [11] S. Li, J. Tang, and C. Yun, "A study on the quantitative remote sensing model for the sediment concentration in estuary," *Acta Oceanol. Sinica*, vol. 24, no. 2, pp. 51–58, 2002.
- [12] W. Ma, Q. Xing, C. Chen, Y. Zhang, D. Yu, and P. Shi, "Using normalized peak area of remote sensing reflectance in the near-infrared region to estimate total suspended matter," *Int. J. Remote. Sens.*, vol. 32, no. 22, pp. 7479–7486, Nov. 2011.
- [13] S. Dai, S. Yang, and A. Cai, "Variation of sediment discharge of the Pearl River basin from 1955 to 2005," *Acta Geographica Sinica*, vol. 62, no. 5, pp. 545–554, May 2007, (in Chinese).
- [14] V. E. Brando and A. G. Dekker, "Satellite hyperspectral remote sensing for estimating estuarine and coastal water quality," *IEEE Trans. Geosci. Remote Sens.*, vol. 41, no. 6, pp. 1378–1387, Jun. 2003.
- [15] Z. Lee, B. Casey, R. A. Arnone, A. Weidemann, R. Parsons, M. J. Montes, B. C. Gao, W. Goode, C. Davis, and J. Dye, "Water and bottom properties of a coastal environment derived from Hyperion data measured from the EO-1 spacecraft platform," *J. Appl. Remote Sens.*, vol. 1, no. 1, Dec. 2007.
- [16] R. Y. Setiawan and A. Habibi, "Satellite detection of summer chlorophyll-a bloom in the gulf of Tomini," *IEEE J. Sel. Topics Appl. Earth. Observ. Remote Sens.*, vol. 4, no. 4, pp. 944–948, Dec. 2011.
- [17] R. K. Sarangi, T. Thangaradjou, A. Saravanakumar, and T. Balasubramanian, "Development of nitrate algorithm for the southwest bay of Bengal water and its implication using remote sensing satellite datasets," *IEEE J. Sel. Topics Appl. Earth. Observ. Remote Sens.*, vol. 4, no. 4, pp. 983–991, Dec. 2011.

- [18] R. Y. Setiawan and H. Kawamura, "Summertime phytoplankton bloom in the south Sulawesi Sea," *IEEE J. Sel. Topics Appl. Earth. Observ. Remote Sens.*, vol. 4, no. 1, pp. 241–244, Mar. 2011.
- [19] M. Lou, Q. Xing, and P. Shi, "Hyperspectral remote sensing for coastal zone and Hyperspectral Imager for the Coastal Ocean," *Remote Sensing Technology and Application*, (in Chinese), to be published.
- [20] H. Shi, Q. Xing, C. Chen, P. Shi, and S. Tang, "Using second-derivative spectrum to estimate Chlorophyll-a concentration in turbid estuarine waters," in *Proc. SPIE, Symp. Remote Sensing and GIS Data Processing and Applications; and Innovative Multispectral Technology and Applications*, Wuhan, China, 2007, vol. 6790, p. 679032.
- [21] Q. Xing, C. Chen, H. Shi, P. Shi, and Y. Zhang, "Estimation of chlorophyll-a concentrations in the Pearl River Estuary using *in situ* hyperspectral data: A case study," *Mar. Technol. Soc. J.*, vol. 42, no. 4, pp. 22–27, 2008.
- [22] Q. Xing, P. Shi, C. Chen, and C. Tang, "Preliminary study on using derivative spectrum to estimate suspended sediments concentration of estuarine waters," in *Proc. 2nd Sino-German Meeting of Joint Steering Committee on Cooperation in Geosciences*, Beijing, China, 2008.
- [23] Landsat Project Science Office. (2006). Landsat 7 Science Data User's Handbook. [Online]. Available: [http://ltpwww.gsfc.nasa.gov/IAS/handbook/handbook\\_toc.html](http://ltpwww.gsfc.nasa.gov/IAS/handbook/handbook_toc.html)
- [24] K. G. Ruddick, F. Ovidio, and M. Rijkeboer, "Atmospheric correction of SeaWiFS imagery for turbid coastal and inland waters," *Appl. Opt.*, vol. 39, no. 6, pp. 897–912, 2000.
- [25] X. M. Xia, Y. Li, H. Yang, C. Y. Wu, T. H. Sing, and H. K. Pong, "Observations on the size and settling velocity distributions of suspended sediment in the Pearl River Estuary, China," *Cont. Shelf Res.*, vol. 24, no. 16, pp. 1809–1826, Oct. 2004.
- [26] R. N. Fraser, "Hyperspectral remote sensing of turbidity and chlorophyll-a among Nebraska Sand Hills Lakes," *Int. J. Remote. Sens.*, vol. 19, no. 8, pp. 1579–1589, 1998.
- [27] J. Tang, X. Wang, Q. Song, T. Li, J. Chen, H. Huang, and J. Ren, "The statistic inversion algorithms of water constituents for the Huanghai Sea and the East China Sea," *Acta Oceanol. Sinica*, vol. 23, pp. 617–626, 2004.
- [28] Z. Lee, C. Hu, R. Arnone, and Z. Liu, "Impact of sub-pixel variations on ocean color remote sensing products," *Opt. Express*, vol. 20, no. 19, pp. 20844–20854, 2012.
- [29] W. D. Philpot, "The derivative ratio algorithm: Avoiding atmospheric effects in remote sensing," *IEEE Trans. Geosci. Remote Sens.*, vol. 29, no. 3, pp. 350–357, May 1991.
- [30] H. Xue and F. Chai, "Coupled physical-biological model for the Pearl River Estuary: A phosphate limited subtropical ecosystem," in *Proc. 7th Int. Conf. Estuarine and Coastal Modeling*, St. Petersburg, FL, USA, Nov. 2001.
- [31] S. Chen, L. Fang, L. Zhang, and W. Huang, "Remote sensing of turbidity in seawater intrusion reaches of Pearl River Estuary—A case study in Modaomen water way, China," *Estuar. Coast. Shelf. S.*, vol. 82, no. 1, pp. 119–127, Mar. 2009.



**Qianguo Xing** received the Master's degree in environmental engineering from South China University of Technology. He received the Ph.D. degree in 2007 from South China Sea Institute of Oceanology, Chinese Academy of Science.

He is an Associate Professor at University of Chinese Academy of Science, and a research scientist at Yantai Institute of Coastal Zone Research, Chinese Academy of Science. His main research interests are coastal environment remote sensing and assessment.



**Mingjing Lou** graduated from Shandong University of Science and Technology with a major in remote sensing and technology in 2010. She is currently a Master's degree candidate at University of Chinese Academy of Science, and works as a research assistant at Yantai Institute of Coastal Zone Research, Chinese Academy of Sciences.

Her research interests are coastal zone mapping and environment remote sensing.



**Chuqun Chen** received the Ph.D. degree in engineering from Lund University, Sweden.

He is a Research Professor at South China Sea Institute of Oceanology, Chinese Academy of Science. His research interest is ocean remote sensing, including atmospheric correction of ocean color satellite image, development of algorithms, validation of ocean remote sensing, remotely sensed assessment of water quality, coastal zone and islands investigation, and thermal remote sensing.



**Ping Shi** graduated from the Shandong Ocean College, China, in 1982, and received the Ph.D. degree from the University of Southampton, U.K., in 1988.

He is a Professor at the University of Chinese Academy of Science, formerly the Director of two institutes at the Chinese Academy of Sciences: Yantai Institute of Coastal Zone Research, and South China Sea Institute of Oceanology. His research interests are ocean remote sensing and physical oceanography.